What influences the water oxidation activity of a bioinspired molecular CoII4O4Cubane? An in-depth exploration of catalytic pathways

Hodel, Florian H ; Luber, Sandra

Abstract: Solar light to chemical energy conversion is an important topic of research due to global climate change and an increasing shortage of fossil fuels. Artificial photosynthesis, as a possible solution to these issues, is strongly dependent on efficient water oxidation. The exact way in which molecular water oxidation catalysts (WOCs), in particular biomimetic cubanes, perform the task of splitting water into oxygen, protons, and electrons still remains unclear to a large extent. We investigated the reaction mechanism of the recently presented first Co(II)-based WOC, [CoII4(hmp)4(-OAc)2(2-OAc)2(H2O)2] (hmp = 2-(hydroxymethyl)pyridine) [Evangelisti, F.; Güttinger, R.; Moré, R.; Luber, S.; Patzke, G. R. J. Am. Chem. Soc. 2013, 135, 18734−18737], which is one of the rare stable homogeneous cubane-type WOCs and the design of which has been inspired by nature's oxygen evolving complex of photosystem II (PSII). Two possible different catalytic cycles have been envisioned: A single-site pathway involving one cobalt center and a water attack on an oxo ligand or, alternatively, an oxo–oxo coupling pathway where, after the replacement of an acetate ligand by water, two terminal oxo ligands of the cubane couple and are released as O2. Using density functional theory and an explicit solvation shell, we compare relative free energies of all states of the catalytic pathways, also with different ligand environments, and analyze the stability and reactivity of each catalytic state in detail. Furthermore, we compute barriers and reaction paths for water attack and O2 release steps. With this knowledge at hand, we propose possibilities to tune catalytic activity paving the way to informed design of high-performance PSII mimics.

DOI: https://doi.org/10.1021/acscatal.5b02507

What Influences the Water Oxidation Activity of a Bio-Inspired Molecular $Co^{II}_4O_4$ Cubane? An In-Depth Exploration of Catalytic Pathways

*Florian H. Hodel and Sandra Luber**

Department of Chemistry, University of Zurich, Winterthurerstrasse 190, CH-8057 Zurich, Switzerland

Abstract: Solar light to chemical energy conversion is an important topic of research due to global climate change and an increasing shortage of fossil fuels. Artificial photosynthesis, as a possible solution to these issues, is strongly dependent on efficient water oxidation. The exact way in which molecular water oxidation catalysts (WOCs), in particular biomimetic cubanes, perform the task of splitting water into oxygen, protons, and electrons still remains unclear to a large extent. We investigated the reaction mechanism of the recently presented first Co(II)-based WOC, [CoII4(hmp)4(μ-OAc)2(μ2-OAc)2(H2O)2] (hmp=2-(hydroxymethyl)pyridine) [Evangelisti, F.; Güttinger, R.; Moré, R.; Luber, S.; Patzke, G. R. *Journal of the American Chemical Society* **2013**, *135*, 18734-18737], which is one of the rare stable homogeneous cubane-type WOCs and the design of which has been inspired by nature's oxygen evolving complex of photosystem II (PSII). Two possible different catalytic cycles have been envisioned: A single-site pathway involving one cobalt center and a water attack on an oxo ligand or, alternatively, an oxo-oxo coupling pathway where, after the replacement of an acetate ligand by water, two terminal oxo ligands of the cubane couple and are released as O_2. Using density functional theory and an explicit solvation shell, we compare relative free energies of all states of the catalytic pathways, also with different ligand environments, and analyze the stability and reactivity of each catalytic state in detail. Furthermore, we compute barriers and reaction paths for water attack and O_2 release steps. With this knowledge at hand, we propose possibilities to tune catalytic activity paving the way to informed design of high-performance PSII mimics.

KEYWORDS: water oxidation • artificial photosynthesis • cubane • density functional theory • oxo coupling • minimum energy path

Introduction

One of the greatest and most important scientific challenges of the 21st century is the increasing global demand for clean energy.[1-3] With the world's energy "consumption" of one year corresponding to the energy delivered by the sun to the earth in one single hour,[4] making use of solar energy is one obvious clean and sustainable solution. Artificial photosynthesis works along these lines by using solar light to split water into molecular oxygen and hydrogen,[5,6] which is a powerful and environmentally friendly carrier for energy storage and conversion. The main efficiency bottleneck of water splitting is water oxidation,[7] characterized by the half-reaction

$$2H_2O \rightarrow O_2 + 4H^+ + 4e^- , \quad (1)$$

$$\Delta G(pH=0, NHE)=113.46 \text{ kcal/mol.}$$

Therefore, a crucial step on the path to commercial implementation of artificial photosynthesis competitive with fossil-fuels is the development of efficient, cheap, and abundant water oxidation catalysts (WOCs) featuring low overpotentials as well as high turnover frequencies and turnover numbers. An obvious starting point for this endeavor is nature's oxygen-evolving complex (OEC), which is part of photosystem II (PSII) where water is oxidized via the so-called Kok cycle.[8-10] It consists of a $CaMn_4O_5$ cluster, which can be thought of as a $CaMn_3O_4$ cubane with a dangling manganese and an oxygen atom bridging it to the cubane,[11-13] surrounded and complexed by several amino acids. The exact structure of the OEC is however still the subject of ongoing research, as is the actual mechanism of O-O bond formation.[14-20] Molecular Mn-oxide catalysts have been designed based on the structural motifs of the OEC, but they do not display significant WOC activity.[21-25]

Starting with Nocera's oxygen evolving catalyst,[26] cobalt oxide has become a subject of interest to many research groups focusing their attention on Co(III)-based cubane type WOCs.[27-31] Wang and Van Voorhis explored a Co(III)-based cubane model complex using a quantum mechanics/molecular mechanics approach investigating an oxo-oxo coupling mechanism.[32] Calculations have also been performed by Li and Siegbahn for a $Co(III)_4O_4$ complex.[33] They found the catalyst to be less active than comparable ones based on manganese due to the increased number of spin crossing events and general energetic aspects. In another computational study, Fernando and Aikens investigated catalytic mechanisms of a Co(III)-cubane WOC and found the lowest energy catalytic states to involve a Co(V)-O radical species.[34] All three of these cubane WOC studies proposed catalytic pathways with different O-O bond formation steps: cross coupling of two oxo ligands [32], nucleophilic attack by a water molecule[33], and geminal coupling of an oxyl radical with a bridging oxygen.[34] Recently, however, it was suggested that Co(III) cubanes suffer from poor stability and that water oxidation catalytic activity is due to Co(II) impurities.[35]

In light of these findings, the first Co(II)-based cubane WOC was reported in 2013 by Evangelisti *et al.*[36] With the goal of

mimicking the structure and functionality of the OEC of PS II, the complex $[Co^{II}_4(hmp)_4(\mu\text{-}OAc)_2(\mu_2\text{-}OAc)_2(H_2O)_2]$ (hmp=2-(hydroxymethyl)pyridine) (**1**) with two bridging and two monodentate acetate ligands as well as two water ligands was synthesized and found to be a stable homogeneous catalyst (see Figure 1). Using $[Ru(III)(bpy)_3]^{2+}$ (bpy=2,2'-bipyridine) as photosensitizer and $S_2O_8^{2-}$ as sacrificial electron acceptor, they measured turnover frequencies which are still far from the standards set by nature and evolution with PSII.[37] Nevertheless, they exceed the ones for comparable catalysts by one or two orders of magnitude.[28,29,38,39] The reasons for the poor performance of artificial WOCs are difficult to determine and catalytic activity depends on many parameters. Nuclearity of clusters, ligand lability, interactions with buffer molecules, as well as the nature of the oxidant can strongly influence catalysis.[40-42] An example for the possibility of tuning WOC activity is a study by Duan *et al.*[40] where they compared two mononuclear Ru-WOCs differing only in the nature of their axial ligands. They found the formation of a Ru-O-O-Ru dimer to be favored by ligands capable of π-π-stacking interactions, which led to that catalyst exhibiting a ten times higher turnover frequency than its analog. As another example, Evangelisti *et al.*[42] were able to improve the catalytic activity of **1** by substituting one cobalt center for a redox inert lanthanide cation.

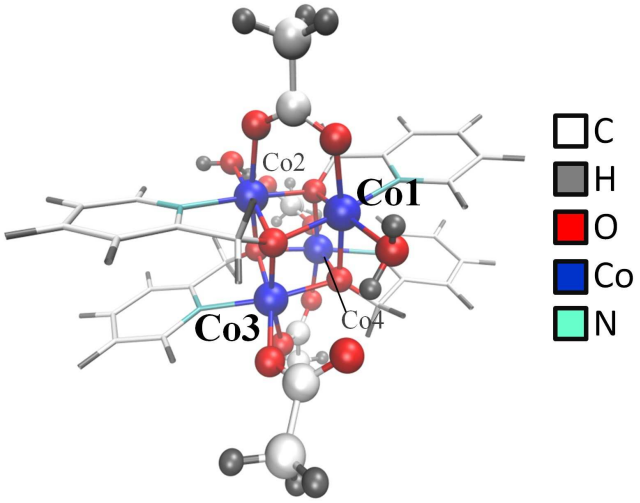

Figure 1. Structure of 1 and numbering of the cobalt centers. The Co-center oxidized during the single-site mechanism is Co1. The ones oxidized during the oxo-oxo coupling pathway (after replacing the monodentate acetate ligand with water) are Co1 and Co3.

Due to its simple and compact structure, **1** represents an excellent model system for the computational in-depth investigation of properties influencing water oxidation activity. Using molecular dynamics (MD) with Kohn-Sham density functional theory (DFT), the nature of its catalytic ground state has recently been extensively investigated showing that the acetate ligands of **1** are thermodynamically stable and ligand exchange with water or hydroxide is unlikely.[42] Tying in on this previous study, we set out to investigate other states of the catalytic cycle of **1** via high-level DFT calculations employing (hybrid) exchange-correlation density functionals and consideration of solvent effects beyond standard solvent continuum models. Together with explorations of minimum energy paths and barriers, this novel approach provides valuable insight into the water oxidation mechanism of **1**, in particular in view of the lack of experimental evidence, and the factors determining its catalytic activity. This is an essential step towards the development of structure-activity relationships and the informed design of high-performance PSII mimics.

Methods

For the geometry optimizations and single point energy calculations of all systems including a solvation shell of 68 water molecules we employed the CP2K package.[43] The coordinates used as a starting point for geometry optimizations of the **S0** states including a solvation shell were derived from a larger DFT-MD equilibrated system (for more details, see below and SI, Methods, Solvation Effects). Calculations of the same systems with the solvent continuum model COSMO[44] instead of explicit solvent molecules were carried out using the program package Turbomole,[45] version 6.5.

For the geometry optimizations, we selected the BP86 exchange-correlation density functional,[46,47] which is known to deliver reliable structures of transition metal complexes.[48-53] Furthermore, single point energies of the optimized structures were determined with the same settings, except for BP86 being replaced with the B3LYP hybrid density functional.[54,56] For calculations with Turbomole, additional geometry optimizations were carried out employing B3LYP instead of BP86. Kwapien *et al.*,[57] investigating model Co(III)-based cubane structures and a single Co-center, found electronic energies calculated with hybrid functionals (B3LYP, PBE0) to agree well with electronic energies obtained with coupled cluster calculations. We repeated all single point energy calculations with the B3LYP* functional[58] and found consistently smaller energy differences between the states of the catalytic cycle than with 20% exact exchange admixed. On average, the energy differences changed by -4 kcal/mol for the single-site pathway and -2 kcal/mol for the oxo-oxo coupling pathway.

Calculations with CP2K used the QUICKSTEP program[59] and mixed Gaussian and plane wave basis sets in combination with (relativistic) Goedecker-Teter-Hutter (GTH) pseudopotentials.[60,61] Additionally, we employed the D3 dispersion correction by Grimme *et al.*[62] which has been shown to be important for transition metal complexes[63] and to arrive at correct reaction energies for water oxidation by an iridium catalyst,[64] as well as a model of the OEC.[49] Cobalt was described by a DZVP-MOLOPT-SR-GTH basis set, whereas all other atom types used DZVP-MOLOPT-GTH.[65] The energy cutoff for the auxiliary plane wave expansion of the charge density was set to 400 Ry which led to the total energy being converged to within 2 meV per atom.

The set-up for the calculations with Turbomole consisted of def2-TZVP basis sets,[66,67] the resolution-of-the-identity density-fitting technique[68] and corresponding auxiliary basis sets,[69] as well as the D3 dispersion correction.

In a previous study we had investigated the dependency of electronic and free energy differences of ligand exchange reactions involving **1** and another Co-based cubane on the

degree of solvation.[42] We had concluded that geometry optimizations with an explicitly represented solvation shell did not necessarily capture all solvent effects and better results had been obtained using DFT-MD sampling. The reason for this lays mainly in the fact that a large geometrical change in the solute (ligand exchange) caused a large structural change in the solvent as well. It can be argued that removal of an electron and proton, as required for the different steps during the catalytic cycle, constitutes a minuscule structural change. We therefore did not expect the minimum energy water shell structure to drastically change during such a reaction. The same is, however, not necessarily true for the attack of a water molecule during the single-site pathway, and this situation warrants closer scrutiny. Nevertheless, we could show with an analysis of the water shell structure that the atomic positions do not significantly change upon water attack (see SI, Figure S5). Furthermore, additional calculations for the **S1**-**S0** energy difference of the single-site pathway starting from completely different solvent geometries did not show significantly varying energetics. The use of implicit solvent models is computationally less expensive and provides "averaged" solvent effects[70] avoiding the need of having the systems to be compared in the same local electronic energy minimum with respect to positions of the solvent molecules. However, it neglects short-range effects such as hydrogen-bonding and reaction energies can vary remarkably depending on the continuum model employed as well as the shape and size of the cavity.[71]

In the catalytic ground state, Co(II) was assumed to be in the quartet spin state[36], coupling ferromagnetically with all other metal centers. Using unrestricted Kohn-Sham DFT calculations, we determined the local minimum energy configuration and the associated electronic energy for all three possible spin states of the oxidized Co-center(s) in the **S1**-**S4** states. The other cobalt atoms were kept in a high-spin state and assumed to couple ferromagnetically, thus requiring no additional spin flips. We justify our choice of this procedure over simply calculating single point energies with different multiplicities from high spin geometries in the SI (Mulliken Spin Populations and Lowest Energy Multiplicities). For the oxo-oxo coupling pathway, we further assumed both oxidized Co-centers, which, apart from the "active" ligand, have the same ligand environments throughout the catalytic cycle, to be in the same spin-state as long as they both carried the same "active" ligand. Therefore, we calculated all possible spin state combinations for state **S3** and for the other states only the above mentioned three spin states. Spin configurations were monitored by Mulliken spin population analysis, i.e. the difference of Mulliken charges for spin-up (α) and spin-down (β) electrons (further details can be found in the SI, Methods, Electronic Structure Methods).

The electronic energy difference ΔE_{i-0} between state **Si** and the catalytic ground state **S0** was calculated for the systems including explicit solvation as

$$\Delta E_{i-0} = E_i + 0.5 i E_{H_2} - E_0 , \quad i = 1, \dots, 4. \qquad (2)$$

E_i denotes the electronic energy of the state **Si**, E_{H_2} the electronic energy of a hydrogen molecule, and E_0 the electronic energy of the catalytic ground state. For the calculations with implicit solvent, this equation needs to be slightly modified (see SI, equation (S1)).

Free energy differences were obtained using an approach introduced by Nørskov *et al.*,[72] which takes advantage of the fact that all steps involve a PCET, and therefore it is only necessary to calculate the free energy of the electron-proton pair, not the individual chemical potential (see SI, Methods, Free energy calculations).

Minimum energy path calculations were carried out using the nudged elastic band (NEB) procedure (see SI, Methods, Minimum energy path calculations).

Results

Water oxidation mechanisms.

In order to investigate the catalytic cycle of oxygen evolution of **1** in detail, we focused on two main pathways: The first one involving only one cobalt center (Co1, see Figure 1 and Scheme 1) and its water ligand, the second oxygen necessarily coming from an attacking water molecule (nucleophilic attack). The second mechanism is an oxo-oxo coupling pathway involving two cobalt centers (Co1 and Co3, see Figure 1 and Scheme 2). While the catalytic ground state for the single-site pathway is exactly **1**, for the oxo-oxo coupling mechanism the acetate ligand on Co3 is replaced by water forming a positively charged complex as ground state. Both pathways consist of four consecutive proton coupled electron transfer (PCET) steps with O_2, 4 H^+, and 4 e^- as products. Figures of minimum energy configurations for every state of both pathways can be found in the SI (Figures S2 and S3).

I. Single-site pathway: The single-site mechanism is initiated by deprotonation of the water ligand and oxidation of Co(II) to Co(III). Repeating this with the second proton gives two resonance structures with different oxidation states on cobalt and the possibility of an oxyl radical, which has been shown for other systems to be more reactive and susceptible to O-O bond formation (see Ref.[73] and references cited therein). Initiating the second part of this pathway, a water molecule attacks forming the desired O-O bond and subsequently, in another PCET step, the system releases one electron and one proton forming a hydroperoxo complex. The last PCET gives Co(IV)(OO) or one of the resonance structures shown in Scheme 1. Finally, O2 is released and after the binding of a water molecule the catalyst has returned to its ground state.

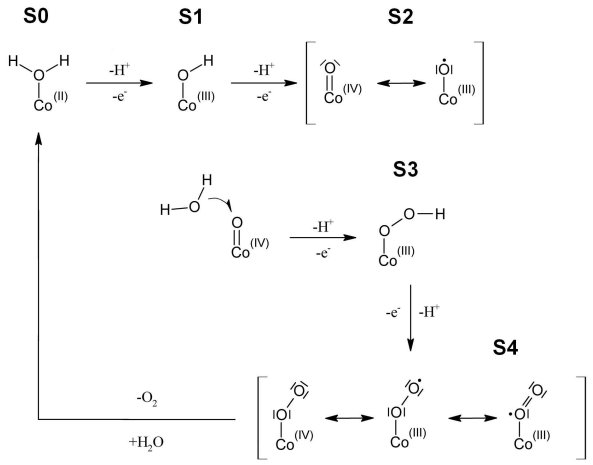

Scheme 1. Single-site pathway.

II. Oxo-oxo coupling pathway: The first step (**S0→S1**) of the oxo-oxo coupling pathway is identical to the one of the single-site mechanism (see Scheme 2). During the second step (**S1→S2**), the transferred proton and electron can either come from the cobalt (and its water ligand) oxidized during step 1, or the other Co-center. Regardless of the nature of the second step, after performing the third one (**S2→S3**), one cobalt ends up with a hydroxo, the other one with an oxo ligand. During the last PCET (**S3→S4**), Co(III)-OH is oxidized to form a second Co(IV)-O. The two oxygen atoms couple, form a bond, and leave the catalyst, which, after association of two water molecules, returns to its ground state.

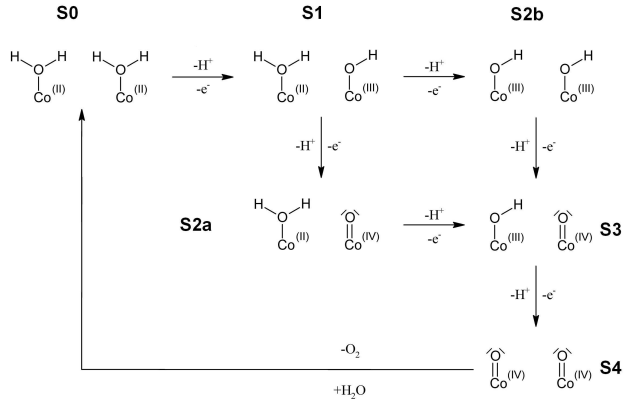

Scheme 2. Oxo-oxo coupling pathway.

As already hinted at in the introduction, these two mechanisms are not the only ones that can be envisioned in general. Yang and Baik[74] proposed a catalytic pathway for a binuclear Ru-complex where the nucleophilic attack of water on an oxo ligand attached to one center is facilitated by interactions with an oxo ligand on the other metal center, which then would also take up the two protons coming from the attacking water. This is reminiscent of a nucleophilic attack on the S4 state of the oxo-oxo coupling pathway, which we investigated and report on below (Alternative mechanisms with different ligand environments). We did not consider a geminal coupling mechanism involving a bridging oxygen atom of the cubane cage as was suggested by Fernando and Aikens for a Co(III) cubane.[34] The reasoning for this is that while their model cubane only had water ligands bound to the Co centers, in **1**, the bridging oxygen atoms have a fourth bond to the hmp ligands, which presumably would render their involvement in a geminal coupling mechanism unfavorable. In a very recent study, Dismukes and coworkers suggested that O-O bond formation involving a $[Co_4O_4]^{5+}$-based "cubium" happens via geminal coupling of two terminal oxo ligands on the same Co center.[75] This event is preceded by partial removal of a bridging bidentate acetate ligand and attack of hydroxide. Their inspiring study certainly motivates future research into the catalytic mechanism of **1**, for which we have already computationally investigated ligand mobility of bridging, as well as monodentate acetate.[42] Finally, we did not consider dimerization of cobalt-oxyl species, as was described for a ruthenium catalyst,[40] due to steric hindrance by the ligands and the absence of experimental evidence for second order kinetics with regard to [**1**].[36,42]

Energy profiles.

The calculated free energy of each state i with respect to the ground state free energy, $\Delta G_{i\text{-}0}$, is shown at the bottom of Figure 2 (only the lowest free energy results in terms of spin multiplicities are shown). We calculated the free energy difference of equation (1) to amount to 102.6 kcal/mol and used it as "computational thermodynamic limit" of water oxidation rather than the experimental value of 113.5 kcal/mol.[76] We are however aware of the (self-interaction) error introduced by calculating molecular oxygen. For both pathways, the third catalytic state already provides enough free energy to oxidize water. The difference between the relative free energy of the **S4** states and the thermodynamic limit describes the free energy released during oxygen evolution (O_2 release, association of water, and structural changes of **1** and the solvent).

According to the Sabatier principle,[77] a "good" catalyst must strike a balance between strong interaction with the substrate, enabling it to bind to the catalyst and being activated, and weak interaction, making it possible for the substrate to dissociate from the catalyst. Thermodynamically, an "ideal catalyst" would have equal free energy differences between its states, making it possible to drive every reaction step with the same minimal potential.[76] The dashed black line in the upper graph of Figure 2 represents the free energy changes of such an "ideal catalyst".[76,78] The relative free energies of the catalyst are scaled by a factor of 113.5 kcal mol^{-1} / 102.6 kcal mol^{-1} = 1.1 to give the experimental value for the free energy change of water oxidation and to account for errors inherent to our approach.[76] While for the oxo-oxo coupling pathway all states are destabilized, the **S1** state of the single-site pathway is slightly over stabilized. **S3** of both pathways is far from the "ideal" catalyst.

Following a simple approach suggested by Nørskov *et al.,* [72,79] we approximated the overpotential by using the largest free energy difference between two consecutive states of the catalytic cycle. For the single-site pathway, this is **S2→S3** ($G(\mathbf{S3})-G(\mathbf{S2})=\Delta G(\mathbf{S2}\rightarrow\mathbf{S3})$=63.1 kcal mol^{-1}) and leads to an overpotential of

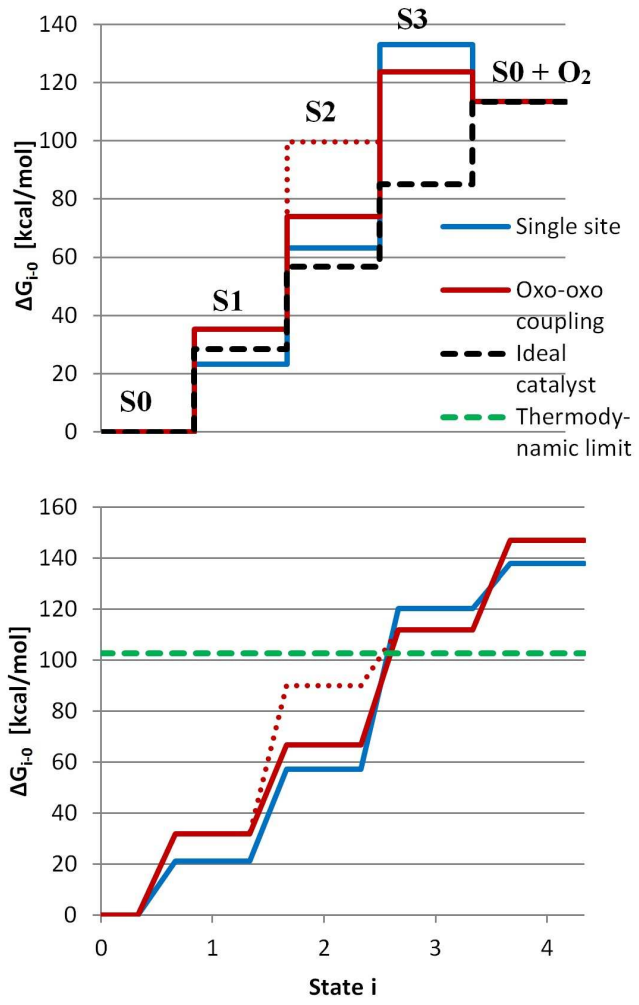

Figure 2. Free energy differences between states of the catalytic cycle and the catalytic ground state. (B3LYP; explicit solvation; for results obtained with other set-ups, see SI, Figure S1 and Table S4). Upper graph: Comparison of the scaled relative free energies of the 4 PCETs with an "ideal" catalyst (dotted black line). Lower graph: Relative free energies of all catalytic states. The dotted red line corresponds to state **S2b**, the thermodynamic limit for water oxidation is not the experimental but the calculated value.

$$\eta_{single} = \Delta G(\mathbf{S2}\rightarrow\mathbf{S3}) - \frac{\Delta G(H_2O,\ pH=0)}{4} \qquad (3)$$

$$= 63.0\ \frac{kcal}{mol} - \frac{102.6\ kcal\ mol^{-1}}{4} = 37.4\ \frac{kcal}{mol} \cong 1.6\ V$$

Similarly, for the oxo-oxo coupling pathway, the largest free energy difference is between **S2a** and **S3**, or, for the alternative second state, between **S1** and **S2b,** resulting in

$\eta_{oxo\text{-}oxo,\ \mathbf{S2a}\rightarrow\mathbf{S3}} = 0.8\ V$ and

$\eta_{oxo\text{-}oxo,\ \mathbf{S1}\rightarrow\mathbf{S2b}} = 1.4\ V.$

For the oxo-oxo coupling pathway, an overpotential of about half the one for the single-site pathway is therefore possible.

Calculations using COSMO instead of explicit water molecules consistently gave lower free energy differences (see Figure S1 and Table S4).

In order to investigate differences in electronic structure between the catalytic states without the influence of zero point energies obtained from vibrational analysis in the harmonic approximation, the electronic energy differences between subsequent states of each of the two pathways are presented in Figure 3. For the oxo-oxo coupling pathway, we show only **S2b** which yields a lower electronic energy difference from **S1** than **S2a**. The *free* energy difference on the other hand, due to the different zero point energies of the two alternative second states (see SI, Table S3), would predict **S2a** to be more favorable as can be seen in Figure 2. The neglect of zero point energies is also responsible for the high electronic energy difference between **S2** and **S1** of the single-site pathway as compared to the free energy difference shown in Figure 2. The electronic energy differences between the lowest energy configurations of the oxo-oxo coupling pathway stay approximately the same from the first to the last state, closely resembling the behavior of an "ideal" catalyst. In contrast to that, the total electronic energy of the system following the single-site pathway increases less when going from **S2** to **S3** than when going from **S1** to **S2**. Although far less pronounced, the energy difference between **S3** and **S4** is again decreased (see Figure 3).

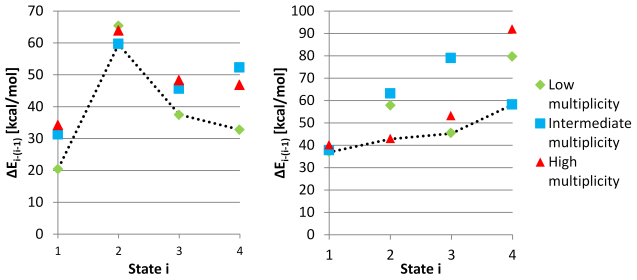

Figure 3. Electronic energy differences between the Si state and the lowest energy configuration of the S(i-1) state (plus half the electronic energy of H_2, compare equation (2)). Computational set-up: B3LYP and explicit solvation. Left: Single-site pathway. Right: Oxo-oxo coupling pathway where only **S2b**, not **S2a**, and only the two lowest and the highest electronic energy configurations of **S3** are plotted.

Influences of spin configurations on the active metal center(s).

The spin configuration on the cobalt metal centers is an important parameter[80] affecting the electronic (and geometric) properties of the WOC and thus the overall WOC activity. We therefore investigated the influence of several spin configurations on the cobalt atoms directly involved in the oxygen evolution in more detail, in particular regarding the energetics during the catalytic cycle.

I. Single-site pathway: As shown in Figure 3 for the single-center pathway, the most favorable electronic configuration of the active cobalt goes from high spin in the catalytic ground state to low spin for **S1** to an intermediate multiplicity of M=13 corresponding to an initial guess of 4 α

and 1 β electrons for the electronic configuration of the active Co for **S2** (see SI, Methods, Electronic Structure Methods). The last two states appear to favor a low spin configuration and also for **S2**, the energy of the low multiplicity system is only a few kcal/mol higher than the lowest one, which means that it could be possible for the mechanism to occur with only one spin crossing event. In any case, the other three cobalt atoms not oxidized during the catalytic cycle were assumed high spin leading to possible values for the total spin multiplicity of M=10, 12, 14 for **S1** and **S3** and M=11, 13, 15 for **S2** and **S4**. The different functionals and solvation methods agree well on the lowest electronic energy multiplicity and differences in atomic positions between multiplicities are small (for details, see SI, Table S1, Figure S6).

II. Oxo-oxo coupling pathway: Here the situation is different, and the two solvation methods predict different spin states to give the lowest electronic energy (SI, Tables S2 and S14). For all states **S1**-**S4** (except for **S2a**, where the deviation is merely 1 kcal/mol), the calculations using the implicit solvent model predict the same multiplicities to give the lowest electronic energies irrespective of the density functional employed. On the other hand, with explicit solvent molecules included in the systems, BP86 and B3LYP differ in their prediction of multiplicity. All methods are, however, consistent with a multiplicity of 10 leading to the lowest electronic energy for the **S1** state (see SI, Tables S2 and S14). For the **S2a** state, the same spin configuration as for the **S2** state of the single-site mechanism is mostly predicted to have the lowest electronic energy. It thus appears that the electronic configurations of the active Co during the first two (**S1**, **S2a**) and the last state (**S4**) are similar to the ones adopted during the single-site pathway. All computational set-ups suggest that at least two spin crossing events take place along the pathway changing the configuration of both active Co-sites from high to low spin one at a time (see SI, Table S14). In terms of catalyst design, one obvious point of improvement is thus the alleviation of those spin crossings. This may benefit from multiple low-lying energy surfaces enabling multi-state reactivity.[81,82]

Spin population and molecular orbital analysis.

I. Single-site pathway: For the single-site mechanism, it appeared that while for **S1** and **S3** there was no spin density accumulated on either ligand oxygen atom, there could be found a significant amount for **S2** and **S4** (compare SI, Tables S5-S8), which is also reflected in the spatial plots of the spin densities (see Figure 4) pointing toward a partial radical character of the oxygen(s), the possibility of which is already hinted at by the resonance structures drawn in Scheme 1. The oxyl radical has been found by many researchers to be an important species in terms of reactivity for water oxidation catalysis.[33,73,83,84]

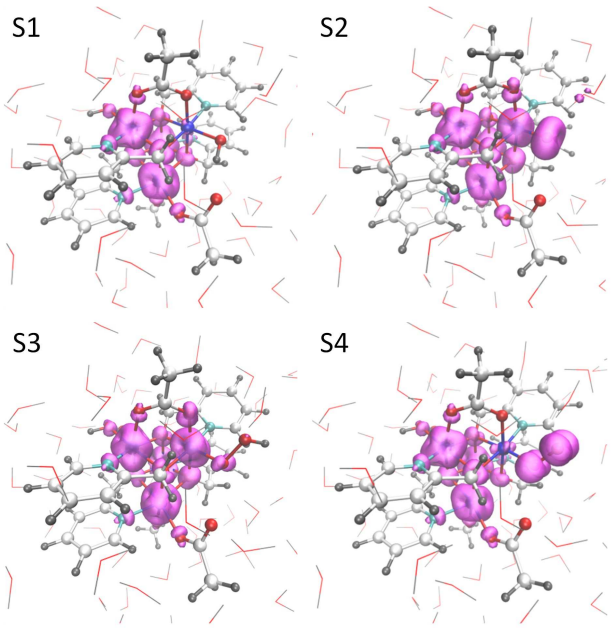

Figure 4. Spin densities for the S1-S4 states of the single-site pathway. Computational set-up: B3LYP and explicit solvation. Isosurface value: 0.005 $Å^{-3}$.

Molecular orbital (MO) analysis further shows that the lowest unoccupied molecular orbital (LUMO) of **S2** is mostly located on the oxyl ligand making it the perfect target for nucleophilic attack by water (see Figure 5, for the frontier orbitals of the other catalytic states see SI, Figure S8 and for results obtained with a different spin multiplicity see SI, Figure S9). A more detailed analysis of interactions of orbitals, occupations of MOs, and their implications for the electronic structure of the **S2** state can be found in the SI (Molecular Orbital and Valence Bond Analysis), where we visualized the radical nature of the **S2** oxo ligand with two 2-center-3-electron π-bonds.

The Co-O_{Ligand} bond lengths were found to be in the range of 1.82-1.86 Å, except for the **S2** state, where the distance from cobalt to the oxo ligand is shortened to 1.65 Å. The cubane-cage changes only slightly during the catalytic cycle. Within the COSMO dielectric continuum, the Co-O_{Ligand} bond lengths are virtually the same as for the explicit solvent systems. The main configurational difference of **1** between the two solvation methods is the position and orientation of the active ligand and the adjacent monodentate acetate in states **S3** and **S4**. The reason for this are most likely the (missing) hydrogen-bonds between water and the monodentate acetate ligand. Within COSMO, the main non-bonding interaction is between the acetate and the changing ligand on the active cobalt (see SI, Figure S4).

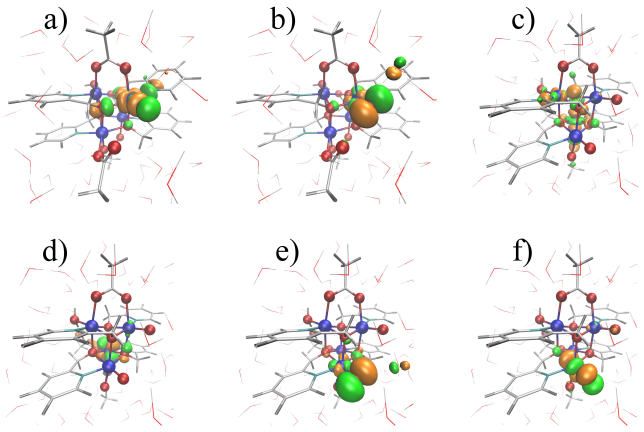

Figure 5. Frontier orbitals. Computational set-up: B3LYP and explicit solvation. a) and b): Single-site pathway, **S2** state, LUMO, α and β spin, respectively. c) and d): Oxo-oxo coupling pathway, **S4** state, HOMO, α and β spin, respectively. e) and f): Oxo-oxo coupling pathway, **S4** state, LUMO, α and β spin, respectively.

The radical character of the OO-ligand in the **S4** state manifests itself in a spin population of approximately 0.5 on either oxygen atom. It is therefore in fact between a superoxo and a molecular oxygen ligand. This goes along with a weakening of the Co-O bond by virtue of shifting electron density into Co-O π*-orbitals[85] as can be seen from Figure S19 in the SI. Hence, increasing this effect should facilitate the release of oxygen and is a toe-hold for tuning the stability of certain catalytic states and thereby the activity of the catalyst itself.

The increased spin population on the ligands is illustrated in Figure 6, where we by no means attempted to accurately depict the energy levels of the orbitals, but rather aimed at clarifying the distribution of electrons between the active cobalt and its ligands in a simplistic way. The scheme shows for each state of the catalytic cycle the cobalt 3d-orbitals, split by an octahedral ligand environment, and the highest occupied molecular orbital (HOMO), or (for the oxo ligand) the highest occupied atomic orbital, of the respective ligand. It is assumed in this picture that no mixing between metal and ligand orbitals takes place, and electrons can be fully assigned to either ligand or metal. In the **S4** state, three electrons occupy the two degenerate π*-orbitals of the superoxo moiety. As mentioned in the previous subsection, in principle, a path involving only one spin crossing event is also energetically plausible and is visualized in Figure 6 (**S2**, dashed arrows).

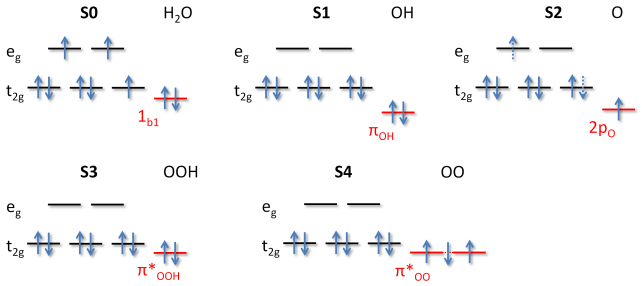

Figure 6. Electronic configuration of the 3d-electrons of Co1 and the HOMOs of the ligand as calculated for the single-site mechanism. Computational set-up: B3LYP and explicit solvation. The dashed arrows for **S2** visualize the energetically close lying low and intermediate multiplicity states with 3 and 4 α electrons on Co, respectively.

Moreover, we found the HOMOs and spin densities mostly to be delocalized over the whole cubane-cage (see Figure 4 and SI, Figures S7-S10). This points toward the important role the cubane plays, as compared e.g. to a single Co^{2+} ion, for the electron transfer and suggests that the electron removed in a PCET is not "local" to the active Co-center.[41] We found no qualitative differences in terms of spin populations between implicit and explicit solvent systems.

II. Oxo-oxo coupling pathway: Plots of spin densities for several low energy systems, as well as tables of Mulliken spin populations for all systems of the oxo-oxo coupling pathway can be found in the SI (Tables S9-S13, Figure S7). As opposed to calculations of the single-site mechanism, the Mulliken spin populations are often reduced on Co atoms other than the active one(s), with COSMO giving, especially for **S3** and **S4**, mostly more localized spin densities than the calculations using explicit solvent molecules. The spin populations located on the two oxygen atoms destined to form O_2, on the other hand, paint a clear picture. The general trend of high spin densities on oxo and low ones on hydroxo ligands, as found for the single-site mechanism, also holds for the oxo-oxo coupling pathway. In particular, the spin populations on the two oxo ligands of **S4** are close to 1 for all methods and all multiplicities. It is worth mentioning that formation of an O-O bond by cofacial oxo ligands has been investigated by Wang and van Voorhis[32] for a Co(III)-based cubane. They have found that the bond is formed by coupling two oxo groups with strong radical character. Similar statements regarding the nature of the oxo ligand have been made by Dismukes and coworkers.[41]

During the oxo-oxo coupling pathway, the Co-O_{Ligand} bond length calculated with explicit water molecules present takes values between 2.01 and 2.05 Å for water ligands (which is longer than for the equivalent state of the single-site pathway), 1.76 – 1.80 Å for hydroxo ligands, and 1.63 – 1.65 Å for the oxo ligands (similar to the single-site mechanism). There are no significant configurational differences between calculations with explicit and implicit solvent, different functionals or different spin multiplicities (see SI, Structural analysis).

As for the single-site pathway, the significant role of the cubane core is underlined by the HOMOs being predominantly positioned on the cubane core (see Figure 5 and SI, Figure S10). Interestingly, the LUMOs of **S2a** and **S2b** are also

partly located on the hmp ligands. Furthermore, while for **S4** there is no electron density associated with the HOMO located on either oxo ligand, the LUMO is mostly located on Co3-O (see Figure 5). However, the LUMO+1, which is only a few kcal/mol higher in energy than the LUMO, is mostly located on Co1-O (not shown).

Alternative mechanisms with different ligand environments.

I. Water attack on the S4 species of the oxo-oxo coupling pathway: In principle, instead of forming O_2 right after **S4** of the oxo-oxo coupling pathway, it is possible to have a water attack followed by a PCET step on either oxo ligand and eventually end up with an oxo ligand on one and (after another PCET) a superoxo ligand on the other cobalt center. This idea is also substantiated by the localization of the LUMO on the oxo ligand(s) (see Figure 5) rendering them prone to nucleophilic water attack. We carried out the calculations of those **S5** (Co1-OOH, Co3-O) and **S6** (Co1-OO, Co3-O) states with implicit solvent (see SI, Table S16). Both steps are thermodynamically plausible to take place in terms of electronic energies. The electronic energy difference between **S4** and **S5**, and **S5** and **S6** amounts to 15.8 kcal/mol and 32.1 kcal/mol, respectively, as compared to 18.8 kcal/mol and 28.5 kcal/mol between **S2** and **S3**, and **S3** and **S4** of the single-site pathway. The difference between the systems can be thought of as substituting Co(II)-acetate neighboring the active cobalt with Co(III)-O for the last two states of the single-site pathway. It should however be kept in mind that since the barriers for the single-site pathway are not lower than the ones associated with the oxo-oxo coupling pathway (see Figures 7, 8, and 9) and two additional PCETs would need to take place, the oxo-oxo coupling pathway is probably the more likely route for the system to take. The spin populations on the ligands as expected, always close to 1 for the oxo ligand (slightly above 1 for **S6**). For the other two oxygen atoms constituting the OO(H)-ligand, the spin populations go from 0 to approximately 0.5. The low spin configuration was mostly favored (for details, see SI, Table S16).

II. Single-site pathway with a different ligand: In order to investigate the influence of the ligand environment for one exemplary case, we calculated electronic energies for the first two states of the single-site pathway with the monodentate acetate attached to Co3 replaced by hydroxide (SI, Table S15). While the electronic energy difference between **S1** and the ground state is larger with the hydroxide ligand than with the acetate ligand, the opposite is true for the electronic energy difference between **S2** and the ground state, which is even 4.5 kcal/mol lower with hydroxide instead of acetate attached. This brings the catalyst closer to a thermodynamically "ideal" one, as can be seen from Figure 2. However, the LUMO and LUMO+1 are located not on the oxo ligand but on the hmp ligands. Presumably, the next step (water attack) is therefore, due to the energetically higher lying accepting orbital, quite difficult. Indeed, also thermodynamically, **S3** with hydroxide attached lies 14.6 kcal/mol further above its ground state than with acetate, which demonstrates that tuning certain catalytic steps might adversely affect others. Nevertheless, after dissociation of the acetate ligand, which is however, as mentioned in the introduction, unfavorable, also a single-site pathway would certainly be an option from a thermodynamic point of view. The energies of the HOMOs are higher with the hydroxide ligand than with acetate, making oxidation easier. It should be mentioned that it was not possible to find a stable geometry for the low spin **S3** state. Irrespective of the initial coordinates, water was formed leaving two oxo ligands behind. Although we did not examine this phenomenon using dynamic methods, it points toward a possible decay of **S3** with a low barrier associated. While the spin populations on the oxygen atom bound to the active cobalt are similar for the acetate and the hydroxide ligand, the ones on the cobalt atoms are not only localized on the oxidized metal, but also on varying other Co-centers, if hydroxide is attached. This is a similar situation as the one found for the oxo-oxo coupling pathway. It appears that the acetate ligand (or rather its replacement with water or hydroxide) has a strong influence on the distribution of electrons over the cubane core structure.

Introducing ligands that facilitate either sterically or electronically the dissociation of the monodentate acetate ligand might benefit catalysis, since not only would this render the oxo-oxo coupling mechanism more favorable (by facilitating the formation of its catalytic ground state), it would also not keep the system from following a single-site pathway. This is reminiscent of a previous study where WOC activity was linked with flexible ligand environment.[42]

Barriers.

The energies discussed up to now focused on the different states of the catalytic cycle without considering the transitions between said states. The latter, though, is indispensable for a thorough understanding of the kinetics and WOC activity as well as the derivation of structure-activity relationships. We assumed the PCET steps to occur very fast and to have only a low energy barrier associated with them. This is also supported by experimental findings on another (nickel-) WOC.[86] For this reason, we focused on the exploration of three transition states: water attack and O_2 release during the single-site pathway and O-O bond formation followed by dissociation of the newly formed oxygen molecule during the oxo-oxo coupling mechanism.

I. Single-site pathway: ***(a) Water attack*****:** The initial guess for the reaction path describing the water attack was generated by moving a water molecule proximal to the active site closer to the oxo ligand of **S2**. Next, one proton was displaced from the attacking water forming a hydronium. In the minimum energy path resulting from the application of the NEB procedure, the proton was further transferred over 3 water molecules (displayed in the "ball-and-stick" representation in Figure 7) forming a hydronium approximately 8 Å from the active site. At the same time, the water molecule turned, breaking the hydrogen bond with the oxo ligand, and the O-O bond formed. This concerted mechanism of proton loss and bond formation has also been found by, for instance, Piccinin *et al.* for a Ru catalyst.[76]

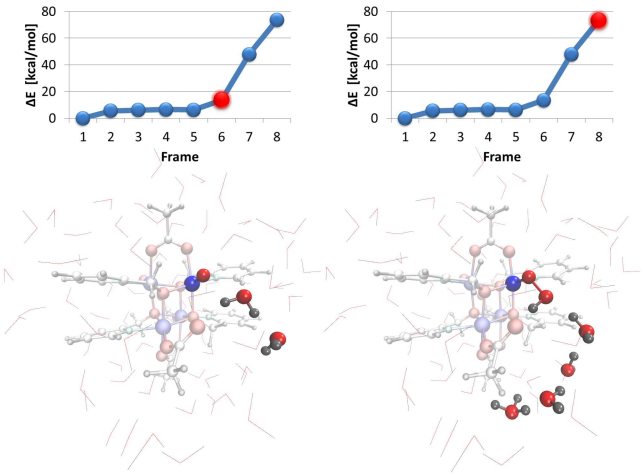

Figure 7. Two NEB-frames of the water attack during the single-site pathway. The electronic energies relative to the first image are marked with a red dot in the graphs above.

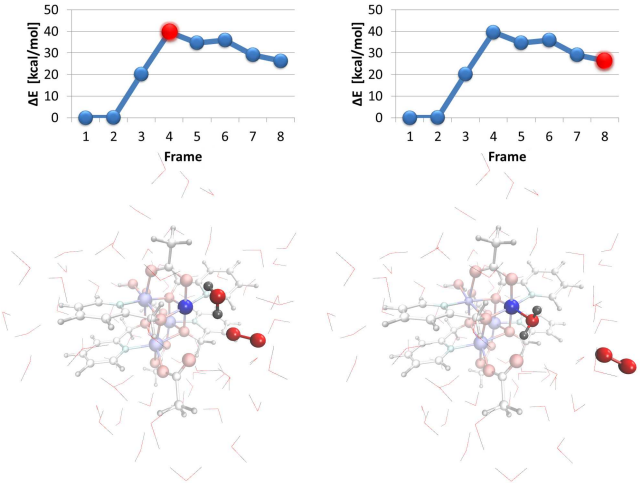

Figure 8. Two NEB-frames of the O2 release during the single-site pathway. The electronic energies relative to the first image are marked with a red dot in the graphs above.

There is no intermediate energy barrier between the first and last frame of the NEB, but with the thermodynamic electronic energy difference between the **S2** and **S3** state of the catalytic cycle amounting to 42.6 kcal/mol, the energy difference between the first and last frame of the NEB (73.5 kcal/mol) can be thought of as the height of the barrier. Except for the active Co1, which returns back to a high spin state after being favorably found with an intermediate spin multiplicity in the **S2** state (see SI, Table S6), the Mulliken spin populations stay the same on the cubane cage over the whole band (see SI, Figures S12, S13, and S16). In agreement with the spin configurations found for the minimum energy configuration of **S3**, the spin population on the oxo ligand is reduced in the last 2 frames during which the O-O bond is formed, whereas the one on Co1 is increased. The next step on the way from **S2** to **S3** is then the removal of one proton from hydronium and one electron from Co1.

For frames 6 and 7, the ones immediately before and after O-O bond formation, we investigated the frontier orbitals (see SI, Figure S11). For the α spin electrons, the HOMO in frame 6 is a nonbonding orbital, whereas the LUMO has σ*-character. For the β spin channel, the HOMO and LUMO are both π*-orbitals lying very close in electronic energy. In frame 7, the attacking water has provided both one α and one β electron going in the σ*- and π*-orbitals, respectively. The α-LUMO of frame 7 is located on one hmp ligand and is far higher in electronic energy than the σ*-orbital. It thus appears that the water attack could be rendered more favorable by lowering the electronic energy of the σ*- (and, if applicable, π*-) orbital (compare SI, Figure S19). This can be achieved, for example, by introducing weaker σ-donating axial ligands.[87-89]

***(b) O_2 evolution*:** The dissociation of O_2 during the single-site mechanism is initialized by a water molecule approaching the active Co1. The transition state, associated with a barrier of 39.6 kcal/mol, corresponds to an incoming water molecule interacting with an oxygen atom belonging to the bridging acetate, as well as with the slightly dissociated O_2 (see Figure 8). Finally, the water attaches to the cobalt and the oxygen molecule drifts away.

The spin populations on the two oxygen atoms constituting the O_2 molecule are always approximately equal (see SI, Figures S12, S14, and S17). The ones on the non-active cobalt centers have the same value except for two frames, which shows how electrons are easily redistributed over the different metal centers of the cubane core during the O_2 formation process. This is even more pronounced for the active Co1 and the attached oxygen atoms, which finally form the O2 molecule in the triplet state (for a detailed discussion, see SI, NEB Calculations).

Concluding, the overall rate limiting step for the single-site pathway appears to be the water attack and O-O bond formation.

II. Oxo-oxo coupling pathway: Our NEB simulation for the O-O bond formation and dissociation of molecular oxygen at the end of the oxo-oxo coupling mechanism led to a minimum energy path with two transition states (see Figure 9). The two oxygen molecules moved closer to each other forming in the second frame an O-O bond bridging the two cobalt centers and constituting the first transition state. Next, the oxygen bound to Co1 detached resulting in O_2 binding to Co3 in a η^2 fashion (frame 3, SI, Figures S12 and S15). A water molecule attached to the now vacant Co1 coordination site, and the OO-ligand changed its hapticity to η^1. This configuration (frame 5, Figure 9) corresponds to a local energy minimum along the path. The next part of the minimum energy path is similar to the one found for the release of O_2 during the single-site mechanism with the exception of the nature of the ligand on the adjacent cobalt, which is now water, as compared to the single-site mechanism, where it was an acetate ligand. The Co3-O bond breaks, O_2 is hydro-

gen-bonding to solvent molecules as well as the previously attached water ligand on Co1, and another water molecule moves in to occupy the vacant coordination site. The transition state of frame 7 corresponds to a configuration where the water molecule is not yet fully attached and the oxygen molecule not fully detached. The height of the first barrier is 41.2 kcal/mol, the one of the second amounts to 32.3 kcal/mol. As for the single-site mechanism, the rate limiting step appears to be the O-O bond formation.

When looking at the evolution of the spin populations along the pathway (see SI, Figure S18), it is evident that again the oxygen atoms forming O_2 always have approximately equal spin populations associated. Furthermore, after the detaching of its oxo ligand, Co1 exhibits a constant high spin population in accordance with a Co(II) state. The spin densities of the other Co centers fluctuate wildly, underscoring that the whole cubane core is electronically involved during the O_2 formation process. As opposed to the study of oxygen dissociation during the single-site pathway, the spin populations on the two oxygen atoms constituting the O_2 molecule in the last frame do not correspond to a triplet oxygen state. This might be, among others, due to the fact that the oxygen molecule is still hydrogen-bonded by the water ligand on Co3 and has not completely drifted away into solution, which should, however, not influence the height of the barrier. We also calculated single point energies of frames 2, 5, 7, and 8 using higher multiplicities than M=9, which was chosen to generate the minimum energy path. This resulted in significantly higher electronic energies than the ones reported for the original NEB calculations.

It is noteworthy that the minimum energy paths are the energetically most favorable ones *close to the initial guess*, depending also on the positions of the explicit solvent molecules, and thus not necessarily the global minimum energy paths connecting two configurations. Approximate transition state energies were therefore additionally obtained with implicit solvent.[90] For the oxygen release steps, we removed the "active" ligand(s) from Co and took the electronic energy difference between the **S4** states and those "transition states" without ligand as approximate barrier heights. For the water attack during the single site pathway, since the height of the barrier appears to be the energy difference between frame 1 and 8, we calculated the electronic energy difference between the cubane at frame 1 plus the attacking and an additional water molecule, and the cubane at frame 8 plus a hydronium ion. These calculations confirmed the trend of barrier height among the investigated paths (for details, see SI, NEB Calculations).

The results of our NEB calculations can only be seen as estimates of the barrier heights due to the above mentioned dependency on the initial guess for the minimum energy path, the neglect of free energy contributions, and the fixed total multiplicity (see SI, Methods, Minimum Energy Path Calculations). Furthermore, during the water attack, it might be more favorable to transfer the proton to a buffer molecule instead of water.[91] Nevertheless, similarly high O-O bond formation barriers have been obtained for a tetranuclear manganese cluster.[92] As pointed out by Liao and Siegbahn, such a reaction could involve excited states and the energy of light might be sufficient to overcome the barriers.[92]

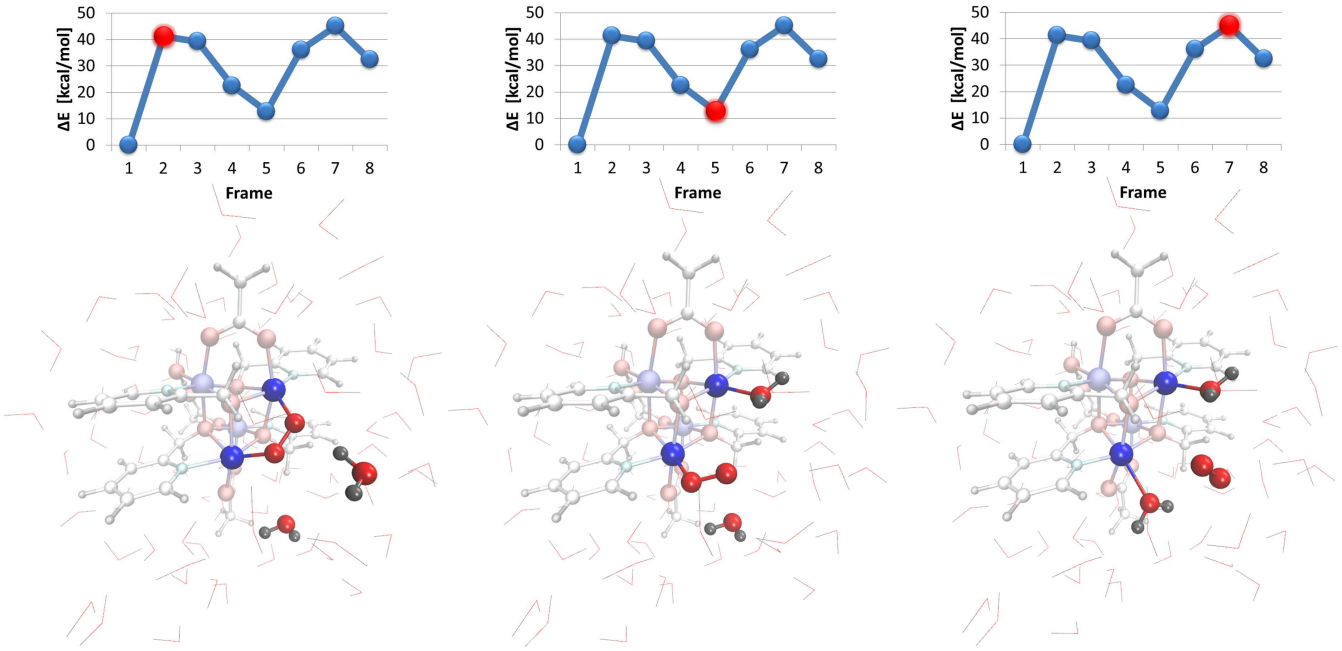

Figure 9. Three NEB-frames of the O-O bond formation and oxygen release at the end of the oxo-oxo coupling pathway. The electronic energies relative to the first image are marked with a red dot in the graphs above.

Conclusion and Outlook

Using high-level DFT calculations, we investigated 2 main water oxidation pathways of $[Co^{II}_4(hmp)_4(\mu\text{-}OAc)_2(\mu_2\text{-}OAc)_2(H_2O)_2]$ (hmp=2-(hydroxymethyl)pyridine), which is one of the rare stable homogeneous cubane WOCs closely resembling the OEC in nature's PSII. As mentioned in the introduction, a major difference between the two catalytic cycles is the necessity to first replace a monodentate acetate ligand with water to arrive at the ground state of the oxo-oxo pathway. We have shown computationally in another study[42] that this acetate ligand is thermodynamically stable. This alone has the potential to render that mechanism slower and in general less favorable.[41] On the other hand, while the oxo-oxo coupling pathway shows thermodynamically, in terms of the energetic "distribution" of its steps, a behavior similar to the single site pathway, as can be seen from Figure 2, it has a lower overpotential and overall energetically lower barriers associated with its catalytic steps. It depends, however, on more spin crossing events taking place than the single-site pathway. For all mechanisms, an important role of the cubane core was encountered as, for instance, observed through the flexible redistribution of electrons over the metal centers during the O_2 formation process. In general, as was exhibited by our catalyst through that distribution of electron and spin density across the cubane cage, stabilization of high oxidation states is very important.[93] Furthermore, for the Co(IV)-O and Co(IV)-OO species, we have found large spin densities and hence strong radical character on the oxygen ligands.

Although systems with implicit and explicit solvation showed similar solute configurations and (for the single-site pathway) similar lowest energy multiplicities and spin populations, the difference in relative free energies of the catalytic states between the two solvation methods was significant. This hints at the necessity of including short-range effects such as hydrogen-bonding but also leads to other issues such as convergence with respect to the size of the solvent shell.

Catalytic activity could, for instance, be increased by facilitating spin crossing events, decreasing the energy of the LUMO of the **S2** state of the single-site pathway, which would make Co-O more prone to nucleophilic attack, labilizing the monodentate acetate ligands, and weakening the Co-OO bond by tuning the π^* orbitals. Already small changes of ligands, such as replacing monodentate acetate with hydroxide or water, led to very different spin densities or localization of frontier orbitals as well as modified energetics of the catalytic states, which is important for the design of an "ideal catalyst" in terms of thermodynamics. Tuning the LUMO of **S2** of the single-site pathway will strongly influence the water attack, which has been found to be the rate-determining step.

Comparing cobalt with manganese, another metal commonly found in water oxidation catalysts, differences have been found concerning electronic structure and reactivity.[33,94] While Co(II) is most commonly found in a high spin configuration, higher oxidation states of Co are often low spin whereas higher oxidation states of Mn exhibit usually still high spin configurations.[95] The weakening of the metal-oxygen bond (mentioned in Spin population and molecular orbital analysis) is more pronounced for Co(IV)-O than for Mn(IV)-O,[85] which has one electron less occupying π-antibonding orbitals compared to low spin Co(IV). Moreover, the LUMO for a water attack at Mn(IV)-O is usually a π^*-orbital, which makes the nucleophilic attack in general sterically more difficult than for the σ^*-LUMO of the Co(IV)-O species.[96]

Aside from redox active metal centers, the influence of redox-inert metal cations, in analogy to the calcium cation in the OEC of PSII, has recently been demonstrated experimentally for $Co(II)_3LnO_4$ (Ln=Ho-Yb) cubanes.[42] The measured improved water catalytic activity would warrant also closer computational scrutiny, as would a further investigation of tuning possibilities by different ligands on the active as well as the other Co centers.

ASSOCIATED CONTENT

All detailed computational methods and results are included in the SI. This material is available free of charge via the Internet at http://pubs.acs.org.

AUTHOR INFORMATION

Corresponding Author

sandra.luber@chem.uzh.ch

Notes

The authors declare no competing financial interest.

ACKNOWLEDGMENT

We thank the National Center of Competence in Research – Materials' Revolution: Computational Design and Discovery of Novel Materials (NCCR-MARVEL) for financial support, and the Swiss National Supercomputing Center (project ID: s502) for computing resources. The work has been supported by the University Research Priority Program "Solar Light to Chemical Energy Conversion" (LightChEC).

REFERENCES

[1] Chow, J.; Kopp, R. J.; Portney, P. R. *Science*, **2003**, *302*, 1528-1531.

[2] Armaroli, N.; Balzani, V. *Angew. Chem. Int. Ed.* **2007**, *46*, 52-66.

[3] Tollefson, J. *Nature* **2011**, *473*, 134-135.

[4] Kärkäs, M. D.; Verho, O.; Johnston, E. V.; Åkermark, B. *Chem. Rev.* **2014**, *114*, 11863-12001.

[5] Lewis, N. S. ; Nocera, D. G. *Proc. Natl. Acad. Sci. USA*, **2006**, *103*, 15729-15735.

[6] Berardi, S.; Drouet, S.; Francàs, L.; Gimbert-Surinach, G.; Guttentag, M.; Richmond, C.; Stoll, T; Llobet, A. *Chem. Soc. Rev.*, **2014**, *43*, 7501-7519.

[7] Young, K. J.; Martini, L. A.; Milot, R. L.; Snoeberger, R. C.; Batista, V. S.; Schmuttenmaer, C. A.; Crabtree, R. H.; Brudvig, G. W. *Coord. Chem. Rev*. **2012**, *256*, 2503-2520.

[8] Joliot, P.; Barbieri, G.; Chabaud, R. *Photochem. Photobiol.* **1969**, *10*, 309-329.

[9] Kok, B.; Forbush, B.; Mcgloin, M. *Photochem. Photobiol.* **1970**, *11*, 457-475.

[10] McEvoy, J. P.; Brudvig, G. W. *Chem. Rev.* **2006**, *106*, 4455-4483.

[11] Ferreira, K.N.; Iverson, T. M.; Maghlaoui, K.; Barber, J.; Iwata, S. *Science*, **2004**, *303*, 1831-1838.

[12] Loll, B.; Kern, J.; Saenger, W.; Zouni, A.; Biesiadka, J. *Nature* **2005**, *438*, 1040-1044.

[13] Suga, M.; Akita, F.; Hirata, K.; Ueno, G.; Murakami, H.; Nakajima, Y.; Shimizu, T.; Yamashita, K.; Yamamoto, M.; Ago, H.; Shen, J-R. *Nature* **2015**, *517*, 99-103.

[14] Dau, H.; Limberg, C.; Reier, T.; Risch, M.; Roggan, S.; Strasser, P. *Chem. Cat. Chem.* **2010**, *2*, 724-761.
[15] Siegbahn, P. E. *Biochim. Biophys. Acta, Bioenerg.* **2013**, *1827*, 1003-1019.
[16] Vogt, L.; Ertem, M. Z.; Pal, R.; Brudvig, G. W.; Batista, V. S. *Biochemistry* **2015**, *54*, 820-825.
[17] Askerka, M.; Wang, J.; Brudvig, G. W.; Batista, V. S. *Biochemistry* **2014**, *53*, 6860-6862.
[18] Cox, N.; Pantazis, D. A.; Neese, F.; Lubitz, W. *Acc. Chem. Res.* **2013**, *46*, 1588-1596.
[19] Petrie, S.; Pace, R. J.; Stranger, R. *Angew. Chem. Int. Ed.* **2015**, *54*, 7120-7124.
[20] Narzi, P.; Bovi, D.; Guidoni, L. *Proc. Natl. Acad. Sci. U.S.A.* **2014**, *111*, 8723-8728.
[21] Tsui, E. Y.; Kanady, J. S.; Agapie, T. *Inorg. Chem.* **2013**, *52*, 13833-13848.
[22] Brimblecombe, R.; Koo, A.; Dismukes, G. C.; Swiegers, G. F.; Spiccia, L. *J. Am. Chem. Soc.* **2010**, *132*, 2892-2894.
[23] Tsui, E. Y.; Agapie, T. *Proc. Natl. Acad. Sci. U.S.A.* **2013**, *110*, 10084-10088.
[24] Wiechen, M.; Berends, H. M.; Kurz, P. *Dalton Trans.* **2012**, *41*, 21-31.
[25] Tsui, E. Y. ; Tran, R.; Yano, J.; Agapie, T. *Nat. Chem.* **2013**, *5*, 293-299.
[26] Kanan, M. W.; Nocera, D. G. *Science* **2008**, *321*, 1072-1075.
[27] McAlpin, J. G.; Stich, T. A.; Ohlin, C. A.; Surendranath, Y.; Nocera, D. G.; Casey, W. H.; Britt, R. D. *J. Am. Chem. Soc.* **2011**, *133*, 15444-15452.
[28] McCool, N. S.; Robinson, D. M.; Sheats, J. E.; Dismukes, G. C. *J. Am. Chem. Soc.* **2011**, *133*, 11446-11449.
[29] Berardi, S.; La Ganga, G.; Natali, M.; Bazzan, I.; Puntoriero, F.; Sartorel, A.; Scandola, F.; Campagna, S.; Bonchio, M. J. *J. Am. Chem. Soc.* **2012**, *134*, 11104-11107.
[30] La Ganga, G.; Puntoriero, F.; Campagna, S.; Bazzan, I.; Berardi, S.; Bonchio, M.; Sartorel, A.; Natali, M.; Scandola, F. *Faraday Discuss.* **2012**, *155*, 177-190.
[31] Symes, M. D.; Surendranath, Y.; Luttermann, D. A.; Nocera, D. G. *J. Am. Chem. Soc.* **2011**, *133*, 5174-5177.
[32] Wang, L.-P.; Van Voorhis, T. *J. Phys. Chem. Lett.*, **2011**, *2*, 2200-2204.
[33] Li, X.; Siegbahn, P. E. M. *J. Am. Chem. Soc.* **2013**, *135*, 13804-13813.
[34] Fernando, A.; Aikens, C. M. *J. Phys. Chem. C* **2015**, *119*, 11072-11085.
[35] Ullman, A. M.; Liu, Y.; Huynh, M.; Bediako, D. K.; Wang, H.; Anderson, B. L.; Powers, D. C.; Breen, J. J.; Abruna, H. D.; Nocera, D. G. *J. Am. Chem. Soc.*, **2014**, *136*, 17681-17688.
[36] Evangelisti, F.; Güttinger, R.; Moré, R.; Luber, S.; Patzke, G. R. *J. Am. Chem. Soc.* **2013**, *135*, 18734-18737.
[37] Stewart, A. C.; Bendall, D. S. *Biochem. J.* **1980**, *188*, 351-361.
[38] Sartorel, A.; Carraro, M.; Scorrano, G.; Zorzi, R. D.; Geremia, S.; McDaniel, N. D.; Bernhard, S.; Bonchio, M. J. *J. Am. Chem. Soc.* **2008**, *130*, 5006-5007.
[39] Car, P.-E.; Guttentag, M.; Baldridge, K. K.; Alberto, R.; Patzke, G. R. *Green Chem.* **2012**, *14*, 1680-1688.
[40] Duan, L.; Bozoglian, F.; Mandal, S.; Stewart, B.; Privalov, T.; Llobet, A.; Sun, L. *Nat. Chem.* **2012**, *4*, 418-423.
[41] Smith, P. F.; Kaplan, C.; Sheats, J. E.; Robinson, D. M.; McCool, N. S.; Mezle, N.; Dismukes, G. C. *Inorg. Chem.*, **2014**, *53*, 2113-2121.
[42] Evangelisti, F.; Moré, R.; Hodel, F.; Luber, S.; Patzke, G. R. *J. Am. Chem. Soc.* **2015**, *137*, 11076-11084.
[43] CP2K Developers Group, URL: http://www.CP2K.org.
[44] Klamt, A.; Schüürmann, G. *J. Chem. Soc. Perkin Trans.* **1993**, *2*, 799-805.
[45] Ahlrichs, R.; Bär, M.; Häser, M.; Horn, H.; Kölmel, C. *Chem. Phys. Lett.* **1989**, *162*, 165-169.
[46] Becke, A. D. *Phys. Rev. A* **1998**, *38*, 3098-3100.
[47] Perdew, J. P. *Phys. Rev. B* **1986**, *33*, 8822-8824.
[48] Bill, E.; Bothe, E.; Chaudhuri, P.; Chlopek, K.; Herebian, D.; Kokatam, S.; Ray, K.; Weyhermüller, T.; Neese, F.; Wieghardt, K. *Cem. Eur. J.* **2005**, *11*, 204-224.
[49] Ames, W.; Pantazis, D. A.; Krewald, V.; Cox, N.; Messinger, J.; Lubitz, W.; Neese, F. *J. Am. Chem. Soc.* **2011**, *133*, 19743-19757.
[50] Orio, M.; Pantazis, D. A.; Neese, F. *Photosynth. Res.* **2009**, *102*, 443-453.
[51] Neese, F. J. *Biol. Inorg. Chem.* **2006**, *11*, 702-707.
[52] Neese, F. *Coord. Chem. Rev.* **2009**, *253*, 526-563.
[53] Neese, F.; Ames, W.; Christian, G.; Kampa, M.; Liakos, D. G.; Pantazis, D. A.; Roemelt, M.; Surawatanawong, P.; Ye, S. F. *Adv. Inorg.Chem.* **2010**, *62*, 301-349.
[54] Becke, A. D. *J. Chem. Phys.* **1993**, *98*, 5648-5652.
[55] Lee, C.; Yang, W.; Parr, R. G. *Phys. Rev. B* **1988**, *37*, 785-789.
[56] Guidon, M.; Hutter, J.; VandeVondele, J. *J. Chem. Theor. Comput.* **2010**, *6*, 2348-2364.
[57] Kwapien, K.; Piccinin, S.; Fabris, S. *J. Phys. Chem. Lett.* **2013**, *4*, 4223-4230.
[58] Reiher, M.; Salomon, O.; Hess, B. A. *Theor. Chem. Acc.* **2001**, *107*, 48-55.
[59] VandeVondele, J.; Krack, M.; Mohamed, F.; Parrinello, M.; Chassaing, T.; Hutter, J. *J. Comp. Phys. Comm.* **2005**, *167*, 103-128.
[60] Goedecker, S.; Teter, M.; Hutter, J. *Phys. Rev. B* **1996**, *54*, 1703-1710.
[61] Hartwigsen, C.; Goedecker, S.; Hutter, J. *Phys. Rev. B* **1998**, *58*, 3641-3662.
[62] Grimme, S.; Antony, J.; Ehrlich, S.; Krieg, H. *J. Chem. Phys.* **2010**, *132*, 154104-154119.
[63] Siegbahn, P. E. M.; Blomberg, M. R. A.; Chen, S.-C. *J. Chem. Theory Comput.* **2010**, *6*, 2040-2044.
[64] Baerends, E. J.; Kazaryan, A. *J. Comput. Chem.*. **2013**, *34*, 870-878.
[65] VandeVondele, J.; Hutter, J. *J. Chem. Phys.* **2007** *127*, 114105-114114.
[66] Weigend, F.; Häser, M.; Patzelt, H.; Ahlrichs, R. *Chem. Phys. Lett.* **1998**, *294*, 143-152.
[67] Weigend, F.; Ahlrichs, R. *Phys. Chem. Chem. Phys.* **2005**, *7*, 3297-3305.
[68] Bauernschmitt, R.; Häser, M.; Treutler, O.; Ahlrichs, R. *Chem. Phys. Lett.* **1997**, *264*, 573-578.
[69] Weigend, F. *Phys. Chem. Chem. Phys.* **2006**, *8*, 1057-1065.
[70] Menucci, B. *J. Phys. Chem. Lett.* **2010**, *1*, 1666-1674.
[71]Ozkanlar, A.; Clark, E. A. *J. Chem. Phys.* **2012**, *136*, 204104-204111.
[72] Nørskov, J. K.; Rossmeisl, J.; Logadottir, A.; Lindqvist, L.; Kitchin, J. R.; Bligaard, T.; Jonsson, H. *J. Phys. Chem. B* **2004**, *108*, 17886-17892.
[73] Khan, S.; Yang, K. R.; Ertem, M. Z.; Batista, V. S.; Brudvig, G. W. *ACS Catal.* **2015**, *5*, 7104-7113.
[74] Yang, X.; Baik, M.-H. *J. Am. Chem. Soc.* **2006**, *128*, 7476-7485.
[75] Smith, P. F.; Hunt, L.; Laursen, A. B.; Sagar, V.; Kaushik, S.; Calvinho, K. U. D.; Marotta, G.; Mosconi, E.; De Angelis, F.; Dismukes, G. C. *J. Am. Chem. Soc.* **2015**, *137*, 15460-15468.
[76] Piccinin, S.; Sartorel, A.; Aquilanti, G.; Goldoni, A.; Bonchio, M.; Fabris, S. *Proc. Natl. Acad. Sci. U.S.A.* **2013**, *110*, 4917-4922.

[77] Sabatier, P. *La Catalyse en Chimie Organique*; Librarie Polytechnique Ch. Béranger: Paris, 1913.
[78] Busch, M.; Wodrich, M. D.; Corminboeuf, C. *Chem. Sci.* **2015**, *6*, 6754-6761.
[79] Nørskov, J. K.; Bligaard, T.; Rossmeisl, J.; Christensen, Ch. *Nat. Chem.* **2009**, *1*, 37-46.
[80] Ritzmann, A. M.; Pavone, M.; Muñoz-Garcia, A. B.; Keith, J. A.; Carter, E. A. *J. Mater. Chem. A* **2014**, *2*, 8060-8074.
[81] Kurashige, Y.; Chan, G. K.-L.; Yanai, T. *Nat. Chem.* **2013**, *5*, 660-666.
[82] Sharma, S.; Sivalingam, K.; Neese, F.; Chan, G. K.-L. *Nat. Chem.* **2014**, *6*, 927-933.
[83] Yang, X.; Baik, M-H. *J. Am. Chem. Soc.* **2006**, *128*, 7476-7485.
[84] Siegbahn, P.E.M.; Crabtree, R.H. *J. Am. Chem. Soc.* **1999**, *121*, 117-127.
[85] Bentley, T. A.; Surendranath, Y.; Childress, M. V.; Allinger, G. E.; Fu, R.; Cummins, C. C.; Nocera, D. G. *Philos. Trans. R. Soc. B* **2008**, *363*, 1293-1303.
[86] Dinca, M.; Surendranath, Y.; Nocera, D. G. *Proc. Natl. Acad. Sci. U.S.A.* **2010**, *107*, 10337-10341.
[87] Bernasconi, L.; Louwerse, M. J.; Baerends, E. J. *Eur. J. Inorg. Chem.* **2007**, *19*, 3023-3033.
[88] Michel, C.; Baerends, E. J. *Inorg. Chem.* **2009**, *48*, 3628-3638.
[89] Ye, S.; Geng, C.-Y.; Shaik, S.; Neese, F. *Phys. Chem. Chem. Phys.* **2013**, *15*, 8017-8030.
[90] Matosziuk, L. M.; Holbrook, R. J.; Manus, L. M.; Heffern, M. C.; Ratner, M. A.; Meade, T. J. *Dalton Trans.* **2013**, *42*, 4002-4012.
[91] Rivalta, I.; Yang, K. R.; Brudvig, G. W.; Batista, V. S. *ACS Catal.* **2015**, *5*, 2384-2390.
[92] Liao, R.-Z.; Siegbahn, P. E. M. *J. Photochem. Photobiol.* **2015**, *152*, 162-172.
[93] Nguyen, A. I.; Ziegler, M. S.; Ona-Burgos, P.; Sturzbecher-Hohne, M.; Kim, W.; Bellone, D. E.; Tilley, T. D. *J. Am. Chem. Soc.* **2015**, *137*, 12865–12872.
[94] McAlpin, J. G.; Stich, T. A.; Casey, W. H.; Britt, R. D. *Coord. Chem. Rev.* **2012**, *256*, 2445-2452.
[95] Young, K. J.; Takase, M. K.; Brudvig, G. W. *Inorg. Chem.* **2013**, *52*, 7615-7622.
[96] Michel, C.; Baerends, E. J. *Inorg. Chem.* **2009**, *48*, 3628-3638.

For Table of Contents Use Only

What Influences the Water Oxidation Activity of a Bio-Inspired Molecular $Co^{II}_4O_4$ Cubane? An In-Depth Exploration of Catalytic Pathways

*Florian H. Hodel and Sandra Luber**